JVI Journals.ASM.org

Structural Insight into African Horsesickness Virus Infection

Violeta Manole,[a] Pasi Laurinmäki,[a] Wouter Van Wyngaardt,[b] Christiaan A. Potgieter,[b]* Isabella M. Wright,[b]* Gert J. Venter,[b] Alberdina A. van Dijk,[c] B. Trevor Sewell,[d] and Sarah J. Butcher[a]

Institute of Biotechnology, University of Helsinki, Helsinki, Finland[a]; ARC-Onderstepoort Veterinary Institute, Onderstepoort, South Africa[b]; Biochemistry Department, North-West University, Potchefstroom, South Africa[c]; and Electron Microscope Unit, University of Cape Town, Cape Town, South Africa[d]

African horsesickness (AHS) is a devastating disease of horses. The disease is caused by the double-stranded RNA-containing African horsesickness virus (AHSV). Using electron cryomicroscopy and three-dimensional image reconstruction, we determined the architecture of an AHSV serotype 4 (AHSV-4) reference strain. The structure revealed triple-layered AHS virions enclosing the segmented genome and transcriptase complex. The innermost protein layer contains 120 copies of VP3, with the viral polymerase, capping enzyme, and helicase attached to the inner surface of the VP3 layer on the 5-fold axis, surrounded by double-stranded RNA. VP7 trimers form a second, T=13 layer on top of VP3. Comparative analyses of the structures of bluetongue virus and AHSV-4 confirmed that VP5 trimers form globular domains and VP2 trimers form triskelions, on the virion surface. We also identified an AHSV-7 strain with a truncated VP2 protein (AHSV-7 tVP2) which outgrows AHSV-4 in culture. Comparison of AHSV-7 tVP2 to bluetongue virus and AHSV-4 allowed mapping of two domains in AHSV-4 VP2, and one in bluetongue virus VP2, that are important in infection. We also revealed a protein plugging the 5-fold vertices in AHSV-4. These results shed light on virus-host interactions in an economically important orbivirus to help the informed design of new vaccines.

African horsesickness (AHS) is a noncontagious, infectious, arthropod-borne viral disease of equids, such as horses and donkeys, that is caused by African horsesickness virus (AHSV) (65). The AHS mortality rate is over 90% in fully susceptible horses (those that have not been exposed to any virus subtype previously), although zebra and African donkeys rarely show clinical signs (16). AHS is endemic to sub-Saharan Africa and the Arabian Peninsula but has periodically caused epidemics in other areas, such as India, Pakistan, Spain, and Portugal (12, 30, 36, 47, 49, 57). The vectors for AHSV are certain species of biting midges in the genus *Culicoides*. Based on the vector's feeding preference for larger mammals, including horses, wide geographical distribution, and relative abundance in light trap collections, *Culicoides* (*Avaritia*) *imicola* Kieffer is considered the most important vector of AHSV in South Africa (45, 69). Oral susceptibility studies coupled to the isolation of AHSV from field-collected midges have also implicated *Culicoides* (*Avaritia*) *bolitinos* Meiswinkel as a potential vector in South Africa (42, 47, 69). The geographical distribution and seasonal incidence of AHS are thus largely determined by the presence of competent *Culicoides* vectors.

In South Africa, AHSV is transmitted by the same insect vectors as those that transmit bluetongue virus (BTV). The presence and spread of BTV in Europe increase the probability that outbreaks of AHS will follow (43, 44, 46, 48, 56, 66). AHS is a World Organisation for Animal Health (OIE)-listed disease, which means that the movement of horses from affected areas is tightly controlled, causing an economic burden on the equine industry in affected countries. A better understanding of the structure and life cycle of AHSV and the mechanisms that control infection in both its insect and equid hosts would inform work on disease control and the development of rationally designed vaccines.

AHSV is a nonenveloped, icosahedrally symmetric virus with a genome composed of 10 linear segments of double-stranded RNA (dsRNA) (5, 53). The species *African horsesickness virus* is classified as a member of the genus *Orbivirus*, within the family *Reoviridae*. There are nine AHSV serotypes (AHSV-1 to AHSV-9) (31, 41). The outer capsid protein VP2 determines the serotype and can induce a protective immune response (7, 10, 39, 62). Eight of the 10 AHSV genome segments code for a single protein (5, 6, 23). There are four nonstructural proteins (NS1, NS2, NS3/3A, and NS4), involved in virus replication, morphogenesis, and release from the infected cell (3, 17, 61, 67, 68). Little is known about the role of NS1 in AHSV replication.

The AHSV particle contains seven structural proteins (VP1 to VP7) arranged as three concentric layers surrounding the genome (5, 6, 23). Only the structure of a proteolytic fragment of VP7 has previously been reported for AHSV (2). The first atomic structure of any orbivirus, that of the BTV 1 core, revealed the organization of the genome and the two innermost layers of the capsid (14, 20, 22). The dsRNA is covered by a shell of 60 asymmetric dimers of VP3, as also seen, for example, in reovirus, rotavirus, L-A virus, and members of the *Cystoviridae* (11, 32, 34, 50, 58, 73). The minor proteins VP1 (polymerase), VP4 (capping enzyme), and VP6 (helicase) form a flower-like transcriptase complex under the 5-fold vertices (51, 61). VP3 is covered by 260 trimers of VP7, organized as a T=13 lattice (14, 20, 22). It has been shown by electron cryomicroscopy (cryo-EM) and image reconstruction that the outermost layer of the BTV virion is formed by the major structural proteins VP2 and VP5, forming triskelions (trimers of VP2) and globular domains on top of VP7 (27, 51, 72). The BTV VP2/VP5 layer mediates cell attachment and entry, determining the replication site of the virus and its cell tropism (18, 19, 25, 26, 70, 72). Although VP2 is believed to mediate the initial cell attach-

Received 7 March 2012 **Accepted** 8 May 2012
Published ahead of print 16 May 2012
Address correspondence to Sarah J. Butcher, sarah.butcher@helsinki.fi.
* Present address: Christiaan A. Potgieter and Isabella M. Wright, Deltamune (Pty.) Ltd., Lyttelton, Centurion, South Africa.
Supplemental material for this article may be found at http://jvi.asm.org/.

doi:10.1128/JVI.00517-12

ment, VP5 contains coiled-coil motifs typical of membrane fusion proteins and is thought to play a role in membrane penetration during cell entry (72).

In this study, we examined AHSV-4 and AHSV-7 tVP2 virions. AHSV-7 tVP2 was shown to have a truncated VP2 protein caused by a deletion in genome segment 2. AHSV-7 tVP2 outgrew the AHSV-4 strain during infection and replication in mammalian cell cultures. We used sequence and structural comparisons of AHSV-4, AHSV-7, and BTV, based on cryo-EM, three-dimensional (3D) reconstruction, and homology modeling, to describe the structure of AHSV and to map two domains in the VP2 structure.

MATERIALS AND METHODS

Virus propagation and purification. The AHSV-4 strain was derived from the OIE reference strain AHSV-4 HS32/62 (16). A freeze-dried stock of the virus was plaque cloned on Vero cells. The AHSV-7 strain was plaque purified from a stock of AHSV-6 (HS39/63) during characterization of stocks for large-scale sequencing and is referred to as AHSV-7 tVP2. AHSV-4 and AHSV-7 tVP2 were produced on BHK-21 cell monolayers and purified on sucrose gradients as previously described (33). Virus was used directly, or samples were lyophilized for storage in 2% (wt/vol) sucrose, 2 mM Tris-HCl, pH 8.5. Purified virus was resuspended in 2 mM Tris-HCl, pH 8.5, at a concentration of 200 μg/ml for AHSV-4 and 50 μg/ml for AHSV-7 tVP2.

Sequencing of AHSV-4 and AHSV-7 tVP2. Extraction of dsRNA from purified virus, sequence-independent genome amplification, high-throughput sequencing, and sequence assembly were performed as described previously (55), using 454 sequencing (Inqaba Biotec, Pretoria, South Africa). Sequence comparison was carried out with online servers for Clustal W for multiple-sequence alignments (21, 35) and with EMBOSS Needle for pairwise alignments (52).

Growth competition experiments between AHSV-4 and AHSV-7 tVP2. A growth competition experiment was set up between AHSV-4 and AHSV-7 tVP2 to see if one of the viruses would outgrow the other. Both viruses were titrated on Vero cells and the stocks diluted to 10^5 50% tissue culture infective doses ($TCID_{50}$) per ml. The stocks were then mixed at ratios of 1:1, 1:10, and 1:100 of AHSV-7 tVP2 to AHSV-4 before infecting Vero cells. The virus mixtures were passaged three times consecutively in Vero cells. Each time, the cells were left until all the cells showed cytopathic effects. After each passage, the cells were harvested, and viral dsRNA was extracted, purified, separated in a 1% agarose gel in Tris-borate-EDTA (TBE) buffer, and stained with ethidium bromide as described previously (55).

Electron cryomicroscopy. Samples were prepared by vitrification of 3-μl aliquots of either fresh or lyophilized and rehydrated virus on Quantifoil R 2/2 holey carbon-coated copper grids as previously described (1). Specimens were held in a Gatan 626 cryoholder maintained at −180°C for imaging in an FEI Tecnai F20 microscope (University of Cape Town) operated at 200 kV under low-dose conditions. Single images were recorded on Kodak SO 163 film at a nominal magnification of ×50,000 (AHSV-4 and empty AHSV-7 tVP2) or on a Gatan Ultrascan 4000 charge-coupled device (CCD) camera at a magnification of ~×83,000 (filled AHSV-7 tVP2). The film was developed in full-strength Kodak D19 developer for 12 min (63).

Image processing. The negatives were digitized using a Zeiss Photoscan TD scanner with a 7-μm step size and were binned to 14 μm. The sampling was done at 0.28 nm/pixel on film and 0.18 nm/pixel by the CCD camera. Micrographs were processed as described previously (63), and the orientations were determined and reconstructions calculated by imposing full icosahedral symmetry using AUTO3DEM (71). The resolution of the reconstructions was estimated by calculating the Fourier shell correlation to 0.5 between two half data sets (24). Visualization and segmentation of the densities were carried out with the UCSF Chimera package (54).

TABLE 1 Statistics of reconstructions

Reconstruction	No. of micrographs	No. of particles	Underfocus range (μm)	Resolution (Å)[a]
AHSV-4	307	1,633	0.8-5.8	14.4
Empty AHSV-7 tVP2	70	361	0.7-4.3	15.8
Filled AHSV-7 tVP2	507	2,798	0.8-4.4	11.4

[a] Fourier shell correlation cutoff of 0.5 (24).

Difference maps between AHSV-4, AHSV-7 tVP2, and BTV 1 (72) were generated in Robem, which is part of the AUTO3DEM package (71). Prior to difference imaging, a low-pass filter with a Gaussian edge was applied to all the reconstructions, using the Bsoft operation bfilter (29) to cut off information beyond 15.8 Å, the calculated resolution of the AHSV-7 tVP2 reconstruction (Table 1).

Modeling of AHSV-4. Structural homology modeling tools were used to make predictions for all of the structural proteins of AHSV-4. The predicted amino acid sequences were submitted to the I-TASSER server (59, 74). Only VP3 and VP7 gave high C scores (0.53 and 1.87, respectively, where the values can range from −5 to 2), indicating models with high confidence (59, 74). These homology models were used to generate an icosahedrally symmetric model of the AHSV-4 core. The BTV X-ray structure of either the VP3 dimer or one monomer of VP7 from the atomic model of the BTV core (RCSB Protein Data Bank [PDB] accession number 2btv) (22) was used to align the corresponding AHSV-4 I-TASSER model, using the Chimera Matchmaker command (54). The resulting pdb file was submitted to the Viperdb oligomer generator to make a pseudoatomic model of the virion core (9). This model was used to disclose the positions of the major proteins VP2 and VP5 and the minor proteins VP1, VP4, and VP6 in Chimera (54).

Accession numbers. The nucleotide sequences obtained in this study were submitted to GenBank under the following accession numbers: for AHSV-7 tVP2, JQ742006, JQ742007, JQ742008, JQ742009, JQ742010, JQ742011, JQ742012, JQ742013, JQ742014, and JQ742015; and for AHSV-4, JQ796724, JQ796725, JQ796726, JQ796727, JQ796728, JQ796729, JQ796730, JQ796731, JQ796732, and JQ796733. The virus reconstructions were deposited in the EMDB database under accession numbers EMD-2075, EMD-2076, and EMD-5412.

RESULTS

The AHSV-4 strain used here came from a plaque from a 1962 field isolate. AHSV-7 tVP2 is a plaque isolate that has a truncated VP2 protein and was identified during large-scale sequencing efforts with AHSV strains at ARC-Onderstepoort Veterinary Institute (ARC-OVI). The dsRNAs of both AHSV-4 and AHSV-7 tVP2 were isolated, and AHSV-7 tVP2 was shown to have a shorter genome segment 2 than those of other AHSV isolates, including AHSV-4 (Fig. 1). Sequencing of genome segment 2 cDNA prepared from the isolate showed that there was an in-frame deletion of the coding region for 225 amino acids in VP2 (residues 279 to 503 are missing). We demonstrated that this deletion in genome segment 2 conveys a competitive advantage on AHSV-7 tVP2 cultured in Vero cells through a growth competition assay where AHSV-4 and AHSV-7 tVP2 were mixed either in equal amounts or with a 10- or 100-fold excess of AHSV-4. In all three cases, after three passages, the AHSV-7 tVP2 strain was dominant as judged by the extracted RNA profile (Fig. 1). Both viruses were purified, and the viral proteins were analyzed by SDS-PAGE. As expected, VP2 from AHSV-7 tVP2 migrated faster than that from AHSV-4, and it can be seen below AHSV-7 tVP2 VP3 on the gel. The profiles for the other viral proteins were very similar (Fig. 2). This natu-

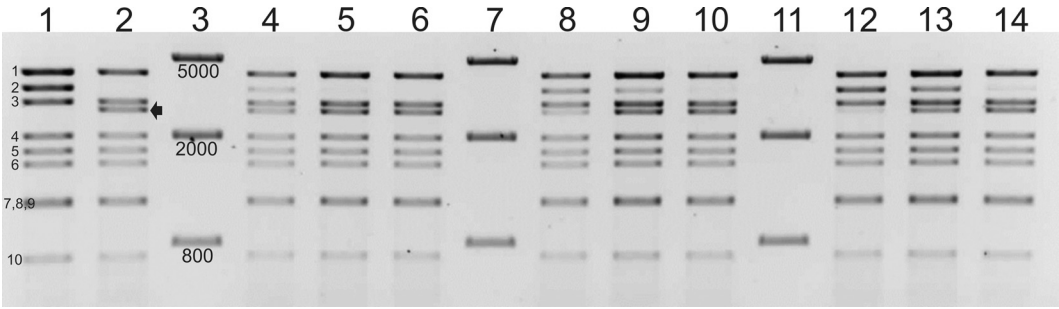

FIG 1 Growth competition in tissue culture between AHSV-4 and AHSV-7 tVP2. Virus stocks of AHSV-4 and AHSV-7 tVP2 were mixed at different ratios and passaged three times in Vero cells. RNAs were extracted, purified, separated in a 1% agarose gel, and stained with ethidium bromide. Lane 1, AHSV-4 dsRNA; lane 2, AHSV-7 tVP2 dsRNA; lane 3, marker; lane 4, 1:1 ratio of AHSV-7 tVP2 to AHSV-4, passage 1; lane 5, 1:1 mixture, passage 2; lane 6, 1:1 mixture, passage 3; lane 7, marker; lane 8, 1:10 ratio of AHSV-7 tVP2 to AHSV-4, passage 1; lane 9, 1:10 mixture, passage 2; lane 10, 1:10 mixture, passage 3; lane 11, marker; lane 12, 1:100 ratio of AHSV-7 tVP2 to AHSV-4, passage 1; lane 13, 1:100 mixture, passage 2; lane 14, 1:100 mixture, passage 3. Genome segments visible on the gel are labeled 1 to 10 in lane 1. The arrow in lane 2 indicates the position of AHSV-7 tVP2 genome segment 2.

rally occurring truncation was a useful tool in our structural analyses. The predicted amino acid sequences of AHSV-4 VP3 and VP7 were used for homology modeling (59, 74).

We analyzed purified samples of AHSV-4 and AHSV-7 tVP2 virus particles by cryo-EM and 3D image reconstruction. The electron micrographs showed that most of the particles from fresh preparations of AHSV-7 tVP2 and AHSV-4 were RNA filled, spherical, and intact, with a diameter of approximately 87 nm (Fig. 3A). The lyophilized samples (AHSV-4 and AHSV-7 tVP2) contained mostly viral particles that had lost the genome, but otherwise they seemed intact (Fig. 3B). Long helical tubules of the nonstructural viral protein NS1, which copurifies with AHSV, were also seen in many of the micrographs (data not shown), similar to those reported for BTV (28).

Reconstructions were calculated from fresh and lyophilized virion preparations, separating the particles into those that were RNA filled and those that were empty. The data sets are summarized in Table 1. The icosahedrally symmetric reconstructions revealed a triple-layered structure encapsidating the 10 dsRNA genomic segments (Fig. 3C and D), as illustrated schematically in Fig. 3E and F. The AHSV-4 and AHSV-7 tVP2 reconstructions are very similar to each other (Fig. 3 to 5). There are three main differences, in the presence of RNA, in the vertices, and in the triskelions. The AHSV-7 tVP2 reconstruction from lyophilized particles lacks the RNA and thus reveals the position of a transcription complex near each of the 5-fold vertices (Fig. 3D, right-hand side, and 6A). The AHSV-7 tVP2 vertices are nonoccluded at the level of VP5 (Fig. 3D and F, 4B and C, and 5K and L), as seen, for example, in BTV (72). However, in AHSV-4, they are occluded by a spherical, poorly defined density (Fig. 3C and E, 4A, and 5G and H). As predicted by the sequencing and protein profiles, the triskelions on the surface of AHSV-4 are considerably larger than those on AHSV-7 tVP2 (Fig. 3C and D, 4, and 7). The VP2 and VP5 layers in both AHSV-4 (mixture of fresh and lyophilized virus) and empty AHSV-7 tVP2 (mainly lyophilized virus) reconstructions appear to have weaker density than that of the VP7 and VP3 layers. We attribute this to partial occupancy of VP2 and VP5, caused by a decrease in the particle structural integrity after lyophilization and rehydration.

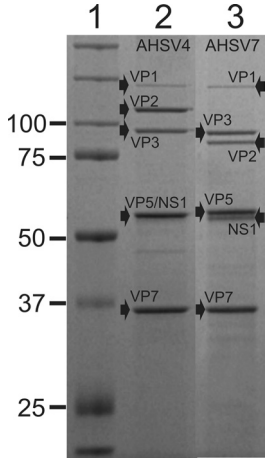

FIG 2 SDS-PAGE analysis of purified AHSV-4 and AHSV-7 tVP2 virions. Virion proteins are marked on the gel, along with the nonstructural protein NS1, which copurified with the virions. A molecular weight standard is shown in lane 1. Comparison of AHSV-4 (lane 2) and AHSV-7 tVP2 (lane 3) clearly shows the difference in molecular weight for VP2.

The innermost shell of AHSV is a T=1 lattice of 60 asymmetric dimers of VP3, which is a flat, approximately triangular molecule of about 103 kDa (Fig. 5A, E, and I and 6A, B, D, and F). The 58% amino acid sequence identity between BTV 1 and AHSV-4 VP3 proteins (Table 2) allowed us to generate homology models for the AHSV-4 VP3 A and B monomers and to align them against BTV VP3 (22, 59, 74). The structures matched very well (root mean square deviations [RMSD] of the α-carbon backbone of 0.2 and 0.3 Å, respectively), with the only difference being the presence of an extra loop and a helix from residues 1 to 59 at the N terminus of the AHSV-4 VP3 A monomer. These homology models were used to generate an icosahedrally symmetric shell that fitted well into the EM density, apart from the first 100 residues of the AHSV-4 VP3 A monomer, indicating that the homology model may be unreliable in this region (Fig. 6F). This is not very surprising, as residues 1 to 56 are missing in the BTV VP3 A monomer atomic model (22), although they were subsequently modeled at low resolution as a chain of density interacting with the transcriptase complexes sitting near each of the 5-fold symmetry axes (20). To be conservative, we removed the first 100 amino acids from the AHSV-4 VP3 A monomer homology model (Fig. 6D). The RNA-filled AHSV-7 tVP2 map shows three well-ordered layers of RNA under VP3 (Fig. 3D, asterisks), surrounding the transcription

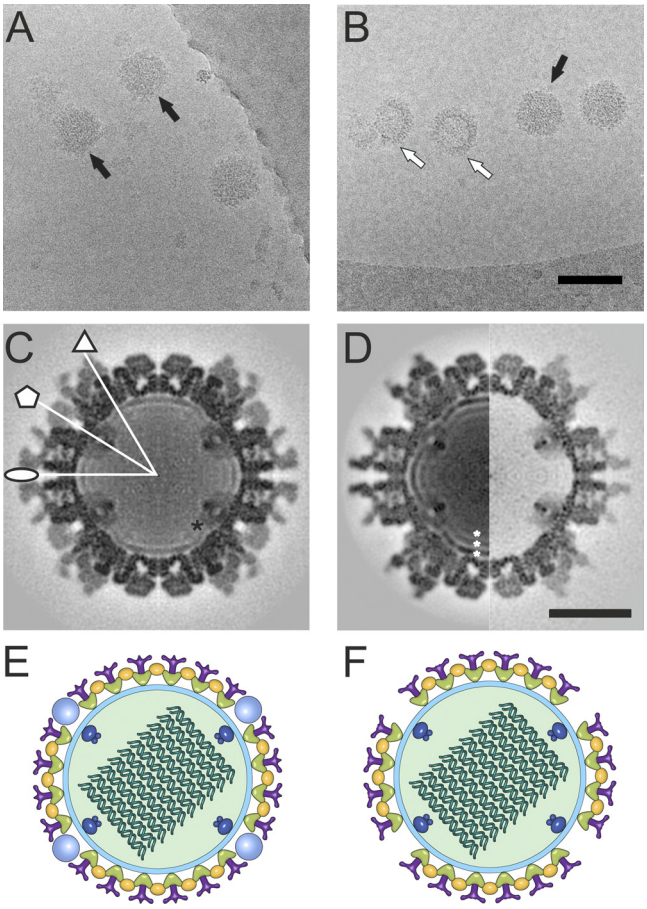

FIG 3 Overall organization of AHSV. (A) Cryo-electron micrograph of AHSV-4, taken with a 1.0-μm underfocus, showing intact viral particles of 87 nm in diameter (black arrows). (B) Cryo-electron micrograph of lyophilized AHSV-7 tVP2, taken with a 1.8-μm underfocus, showing intact viral particles (black arrow) and ones devoid of RNA (white arrows). Bar, 100 nm. (C) Central cross section through the AHSV-4 reconstruction (0.28 nm thick). Twofold (ellipse), 3-fold (triangle), and 5-fold (pentagon) axes of symmetry are indicated. (D) Central cross section through the AHSV-7 tVP2 reconstructions from filled (left; 0.18 nm thick) and empty (right; 0.28 nm thick) particles. Three well-ordered layers of RNA (white asterisks) are indicated. Bar, 25 nm. Proteins are black. (E and F) Schematic organization of AHSV-4 (E) and AHSV-7 tVP2 (F), showing genomic RNA segments (forest green strands) and polymerase complexes (dark blue) enclosed by VP3 (cyan). Trimers of VP7 (green) attach to the surface of VP3. Trimers of the serotype determinant VP2 (purple) sit directly on top of VP7, with VP5 trimers (yellow) filling the spaces of the VP2 lattice. The AHSV-4 virion has additional density on the surface, from an unidentified protein (pale blue circles in panel E).

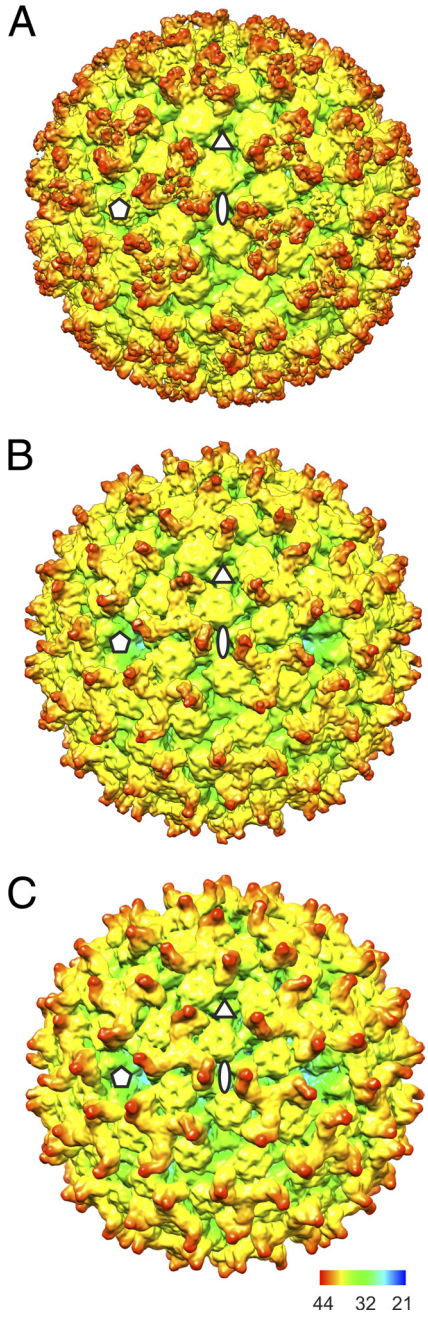

FIG 4 Radially depth-cued isosurface representations of the reconstructions, viewed down a 2-fold axis of symmetry. The isosurfaces were drawn at 1 σ above the mean density level. The structures were radially depth cued in Chimera (54). (A) AHSV-4 at 14.4-Å resolution; (B) empty AHSV-7 tVP2 at 15.8-Å resolution; (C) filled AHSV-7 tVP2 at 11.4-Å resolution. The radial depth-cueing scale bar shows scale in nm. Fivefold (pentagon), 3-fold (triangle), and 2-fold (ellipse) symmetry axes are marked on each representation.

complexes. The spacing between the ordered RNA layers is 3 nm. There are shallow grooves in the inner surface of BTV VP3, along which RNA can move, and these were also seen in the AHSV reconstructions and homology models (20, 22). Although the dsRNA genome is organized as 10 unique linear segments, the individual segments were icosahedrally symmetrized during the reconstruction, thus smearing the density and making them indistinguishable.

The next capsid shell, representing the surface layer of the AHSV core particle, is composed of 780 monomers of VP7 (38 kDa), arranged as 260 trimers on a T=13 lattice (Fig. 5B, F, and J and 6A, C, and G). A homology model of the full-length AHSV-4 VP7 monomer (an X-ray structure is available for the top domain [2]) was generated with very high confidence and an RMSD compared to BTV of 0.5 Å (Fig. 6E), which fitted well into the corresponding EM density for all three reconstructions (Fig. 6).

The outermost layer of the virion (Fig. 3, 4, 5D, H, and L, and 7; also see Fig. 8) is formed by the major structural proteins VP5 (57 kDa) and VP2 (124 kDa for AHSV-4). The major difference in

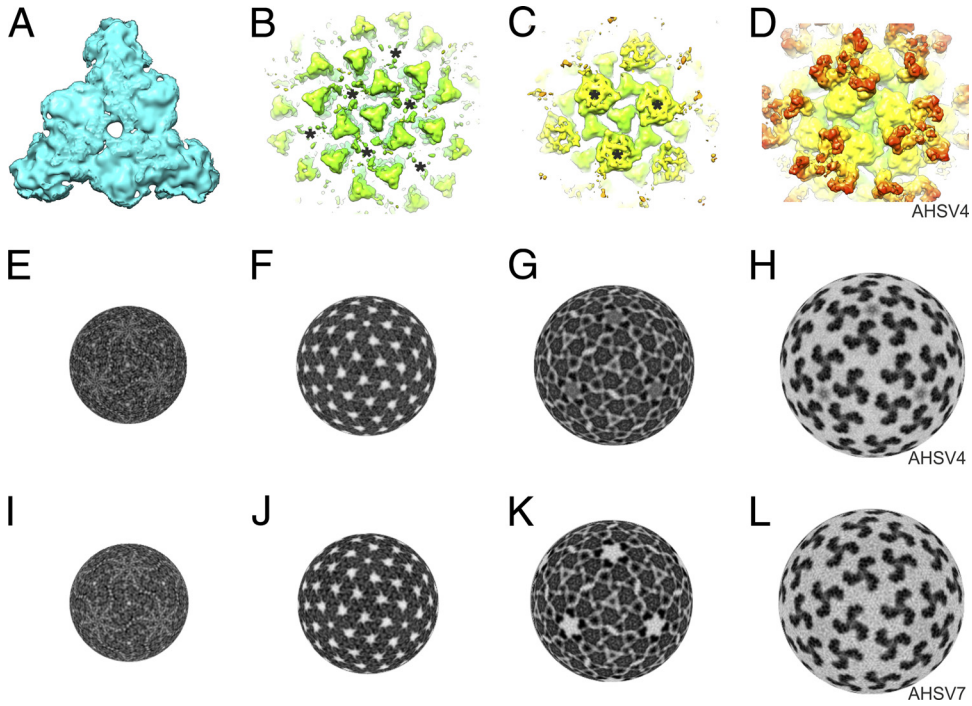

FIG 5 Comparison of protein layers within the structures of AHSV-4 and AHSV-7 tVP2, looking down a 3-fold axis of symmetry. (A) Three molecules of VP3 from AHSV-7 tVP2 are shown at a threshold of 1 σ above the mean. The density was cut out using a 12-Å zone radius around the homology model of a VP3 trimer fitted into the density in Chimera (54). (B) AHSV-4 shown at a threshold of 3.2 σ above the mean so that the organization of the green VP7 trimers is evident. (C) AHSV-4 shown at a threshold of 2.5 σ above the mean so that the organization of VP7 with the intervening VP5 trimers (yellow) sitting on the quasi-6-fold axes of symmetry (indicated with black asterisks in panels B and C) is evident. (D) AHSV-4 shown at a threshold of 1 σ above the mean so that the organization of VP2 (red) is evident. (E to L) Radial shells of the AHSV-4 and AHSV-7 tVP2 reconstructions. Proteins are black. (E to H) AHSV-4; (I to L) AHSV-7 tVP2. (E and I) VP3 layer at 26.2-nm radius; (F and J) VP7 trimers visible at 29.4-nm radius; (G and K) VP5 trimers visible at 35.3-nm radius, where the additional density plugging the 5-fold vertices in AHSV-4 is obvious compared to the case in AHSV-7 tVP2, which has holes on the 5-fold vertices; (H and L) VP2 triskelions at 38.9-nm radius.

the reconstructions between AHSV-4 and AHSV-7 tVP2 is the size of the triskelions that are centered directly on top of the VP7 Q trimer (22, 72). These 60 triskelions, formed from 180 copies of VP2, are much smaller in AHSV-7 tVP2 (Fig. 3, 4, and 7). By amino acid sequence comparison of 24 related proteins from AHSV, BTV, and epizootic hemorrhagic disease virus, it was possible to align the deletions in AHSV-7 tVP2 and BTV 1 with the AHSV-4 sequence (Fig. 7A; see Fig. S1 in the supplemental material). VP2 is the least conserved among the AHSV and BTV structural proteins (Table 2); for example, there is only 40% identity in this protein between AHSV-4 and AHSV-7 tVP2 in a pairwise alignment, with only 17% identity between AHSV-4 and BTV 1 (52). Since VP2 is the major immunogen, it is highly variable due to selective pressure from the host immune system. Thus, we carried out superimpositions of the VP2 triskelions from AHSV-4, AHSV-7 tVP2, and BTV 1 to identify approximately where amino acids 279 to 503 lie in the AHSV-4 VP2 3D structure. Two main differences were seen, one in the tips (tip domain) and the other in the center of the triskelion (central domain) (Fig. 7E and F). The central domains are lacking from both BTV 1 and AHSV-7 tVP2 VP2 molecules, as can be seen in Fig. 7C and F. One domain presumably comes from one VP2 monomer. Each central domain thus corresponds approximately to VP2 residues 368 to 483 in AHSV-4 (Fig. 7A). The distal tips of the triskelions are lacking only from AHSV-7 tVP2. This difference is evident when AHSV-7 tVP2 is compared to either AHSV-4 or BTV 1 (Fig. 7C, D, F, and G). This tip density thus comes primarily from residues 279 to 368 in AHSV-4 (Fig. 7A). Hence, the triskelion wings are positioned in the N-terminal direction from the central domain.

VP5 is a globular trimeric protein positioned in two different environments, i.e., between the peripentonal VP2 molecules and around VP7 on the 3-fold axis of symmetry (Fig. 4 and 5C, G, and K). In both environments, VP5 is in close proximity to VP2. It is predicted to be mainly α-helical (data not shown). Comparison of VP5 proteins segmented from the BTV 1 and AHSV-7 tVP2 reconstructions (72) indicated that AHSV VP5 is very similar to that of BTV 1 in shape, and probably also in fold topology, even though it was not possible to make a reliable homology model of AHSV VP5 to confirm this independently (Fig. 8).

DISCUSSION

AHS is endemic to the African continent, and due to recent events with BTV, it is considered a potential threat to horses in southern Europe. It has previously caused outbreaks in Spain (1987 to 1990) and Portugal (1989), causing major economic losses in the equine industry (12, 47). We have determined the sequences and architecture of AHSV-4 and AHSV-7 tVP2, belonging to the genus *Orbivirus* in the family *Reoviridae*, using cryo-EM and 3D image reconstruction. We observed marked structural similarities between AHSV and BTV (the type species of the family), especially in their core particles (14, 20, 22, 72). This helped in interpreting the AHSV data.

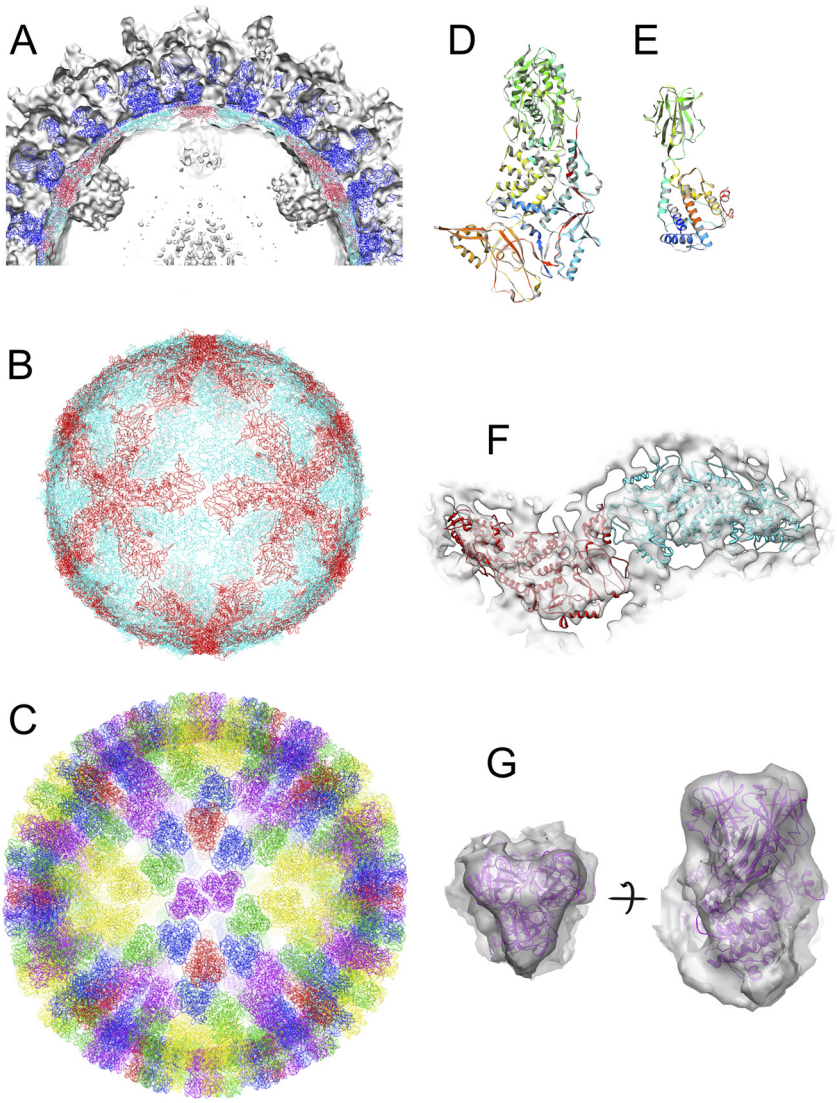

FIG 6 Modeling of VP3 and VP7. (A) Slabbed isosurface representation of the AHSV-7 tVP2 empty-particle reconstruction, rendered at 1 σ above the mean with the fitted homology models of VP3 (cyan and red string) and VP7 (blue string). The densities correspond very well. The transcription complexes can be seen as protruding lumps of density beneath VP3 penetrating into the interior of the capsid. (B) Homology model of the VP3 shell, containing 120 molecules in a T=1 arrangement. The two copies of VP3 within one asymmetric unit are colored cyan and red. (C) Homology model of the VP7 shell, containing 780 molecules in a T=13 arrangement. The asymmetric unit contains 13 copies of VP7. The 5 trimers (P, Q, R, S, and T) contributing to the asymmetric unit are colored yellow, green, blue, purple, and red, respectively (nomenclature according to reference 22). Trimer T sits on an icosahedral 3-fold axis, so it contributes only one monomer to the asymmetric unit. (D) Superposition of the AHSV-4 VP3 A monomer homology model on the BTV VP3 A monomer (22), using ribbon representation. (E) Superposition of the AHSV-4 VP7 homology model on the BTV VP7 A monomer (22), using ribbon representation. AHSV-4 VP3 and VP7 are colored from the N terminus (blue) to the C terminus (red), according to amino acid sequence. BTV VP3 and VP7 are presented as gray ribbons. (F) Homology model of a VP3 dimer (cyan and red) fitted into the EM density of the VP3 shell from filled AHSV-7 tVP2 (gray isosurface), shown at a threshold of 1.7 σ above the mean. The density was cut out using a 20-Å zone radius around the homology model, using Chimera (54). (G) Homology model of a VP7 trimer (magenta) fitted into the EM density of the VP7 layer from empty AHSV-7 tVP2 (gray isosurface), shown at a threshold of 1.9 σ above the mean, from the top and from the side. The density was cut out using a 14-Å zone radius around the homology model, using Chimera (54).

Homology modeling and fitting of AHSV-4 VP7 and the asymmetric dimer of VP3 indicated that the inner core has a similar topology to that of BTV 1 (22). The AHSV-4 and AHSV-7 tVP2 VP3 layers were closed at their 5-fold vertices, preventing the escape of nascent RNA, which is thought to exit through there during active transcription in BTV (14, 22). In addition, AHSV-4 had an additional density blocking the 5-fold vertices at the level of the VP5 shell. This protein is probably incorrectly 5-fold averaged or flexible, as the structure does not show the same level of detail for this protein as for the rest of the proteins. Given the size of this density, it could be a trimer of VP5 which has been smeared by 5-fold averaging applied during the reconstruction process, or it could be part of VP2 from the surrounding triskelions.

VP2 is the major determinant of the immune response to AHSV, raising neutralizing antibodies in infected or vaccinated animals (10, 15, 39, 60, 62, 64). As such, it is subject to selective pressure from the equid host, yet it must maintain its function (and thus structure), as it plays a critical role in the initial steps of

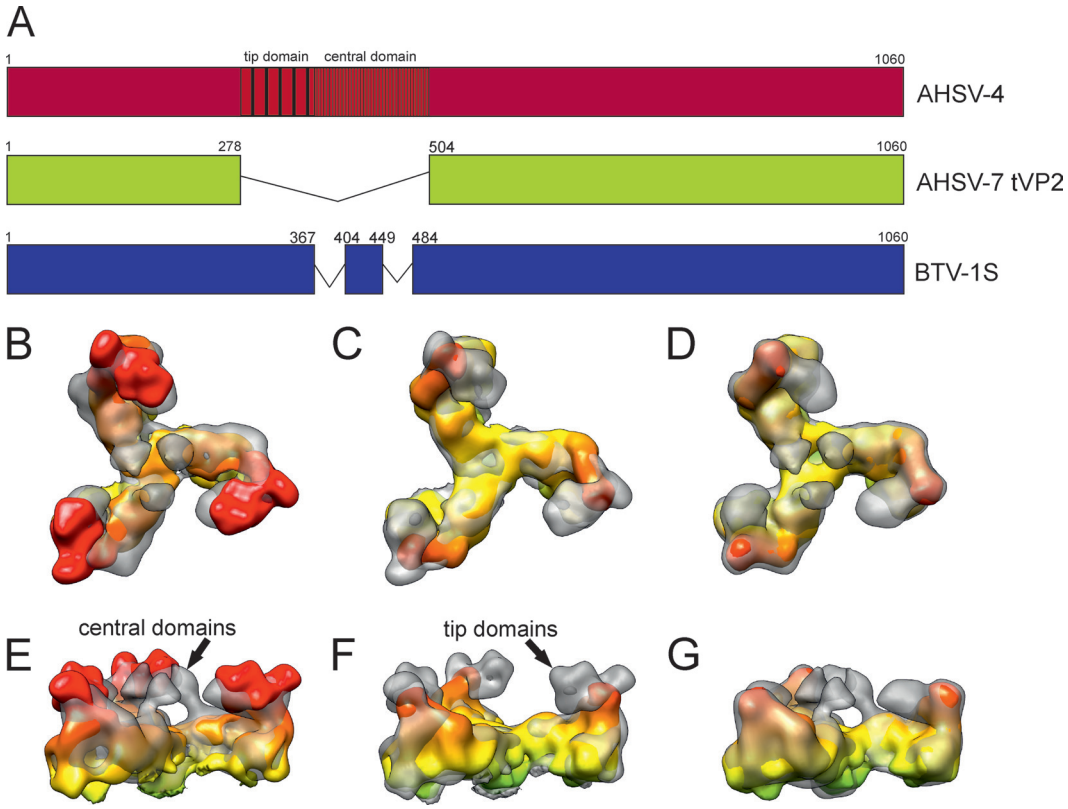

FIG 7 Mapping of deletions in VP2. (A) Schematic showing the positions of the major deletions in AHSV-7 tVP2 and BTV 1 compared to AHSV-4 obtained from a multiple-sequence alignment (see Fig. S1 in the supplemental material). Numbers indicate amino acid residues according to the AHSV-4 sequence. (B and E) Superposition of VP2 proteins from AHSV-4 (gray transparent density) and BTV (radially depth-cued density), from the top (B) and from the side (E). The main additional density in AHSV-4 is in the center of the triskelion on top of the hub, coming from residues 368 to 483 in AHSV-4. (C and F) Superposition of VP2 proteins from BTV 1 (gray transparent density) and the empty AHSV-7 tVP2 reconstruction (radially depth-cued density), from the top and from the side. The main additional density is in the distal end of the triskelion coming from residues 279 to 367 in BTV 1 and AHSV-4. (D and G) Superposition of VP2 from AHSV-4 (gray transparent density) and AHSV-7 tVP2 (radially depth-cued density), from the top and from the side. The main additional densities are in both the center and the distal ends of the triskelion coming from residues 279 to 367 and 368 to 483 in AHSV-4.

infection. VP2 is sensitive to equine serum proteases, which increase the infectivity of the virus in *Culicoides variipennis* (8, 38). It is highly likely that VP2 endoproteolytic cleavage can also occur in the saliva of the insect host, as has been demonstrated for BTV (13). Thus, VP2 activation could play a crucial role in virus entry *in vivo*, as a host specificity determinant. Hence, knowledge of VP2 structure and changes occurring in VP2 that affect infectivity is important in guiding the development of possible vaccines (10).

We report an AHSV-7 strain that has a deletion of 225 amino acids (residues 279 to 503) in VP2 compared to AHSV-4 VP2, in a region that is known to contain immunogenic epitopes (4, 39). Amino acids 340 to 360 have been implicated in determining tissue tropism and virulence (55). Here we demonstrated that the AHSV-7 tVP2 strain outgrows AHSV-4 in tissue culture and also

TABLE 2 Percent identity between amino acid sequences of the viruses used for structural comparison

Viral structural protein	% Identity between viruses		
	AHSV-4 and BTV 1	AHSV-7 and BTV 1	AHSV-4 and AHSV-7
VP1	55.73	55.73	98.39
VP2	17.12	17.06	40.04
VP3	58.02	58.02	99.67
VP4	50.39	50.39	98.60
VP5	42.31	41.56	80.79
VP6	30.08	31.59	62.67
VP7	43.06	42.46	99.71

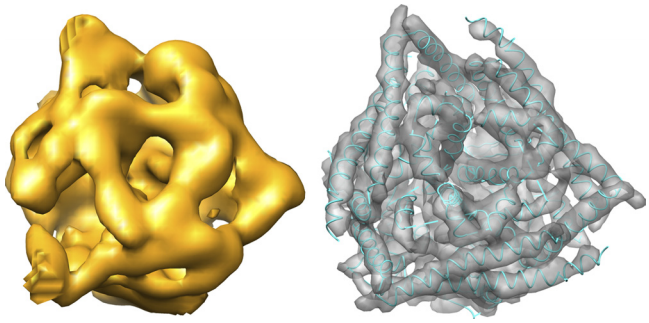

FIG 8 Comparison of VP5 from the AHSV-7 tVP2 empty-particle reconstruction and from a BTV-1 reconstruction (72). The VP5 densities were segmented from their respective reconstructions in Chimera (54). The AHSV-7 tVP2 protein is shown as a gold isosurface, and the BTV protein is shown as a gray transparent solid (EMDB accession code 5147), with blue wire showing the C-α backbone of VP5 (PDB accession code 3IYK).

that infected cells show full cytopathic effect faster, implying that it may have a selective growth advantage. We took advantage of the shorter VP2 protein to locate the above-mentioned residues in an AHSV-4 reconstruction by comparison to AHSV-7 tVP2 reconstructions. We mapped amino acids 279 to 368 onto the AHSV-4 structure and showed that these immunogenic epitopes are most probably located on the tips of the VP2 triskelions, free from interaction with VP5 or VP7 and thus easily subject to mutation (Fig. 7). We also roughly mapped the other major immunogenic residues of AHSV-4 VP2 (amino acids 368 to 403 and 450 to 483) (4) to the top of the triskelion hub (central domain in Fig. 7B, E, D, and G). It is likely that the actual central domain is made of fewer residues than this. We propose that the central domain is a good potential target for the horse serum protease (8, 38), as it sits on top of the putative sialic acid binding site identified in the BTV 1 hub (72). It is absent from both BTV 1 and AHSV-7 tVP2; hence, increased accessibility to the putative receptor binding site could explain the observation of faster growth of AHSV-7 tVP2 than of AHSV-4. In the future, reverse genetics should be applied to make specific deletions in this region in an otherwise homogeneous background to test this hypothesis (40).

Secondary structure prediction of AHSV VP5 indicates that this mainly α-helical protein has an N-terminal amphipathic helical region (residues 1 to 41 in AHSV-4) (data not shown) which is a potential fusion peptide (37). Thus, one likely series of events for cell entry of the virion is as follows: proteolytic cleavage of VP2 in the serum or in midge saliva, interaction with the host cell receptor, entry through an endocytic pathway, low-pH activation of VP5 leading to exposure of the fusion peptide and its insertion into the endosomal membrane, and release of the double-shelled core into the cytoplasm, as suggested for BTV (18, 19, 72).

In conclusion, the AHSV structures are the starting point for a fuller understanding of the interaction of VP2 with host cells and the effects of host-driven evolution of the virus to escape the immune responses of both midges and horses. This is extremely important for the development of better, more efficient vaccines. In the future, reverse genetics, an atomic model of VP2, mapping of the serum protease sites, and detailed cell biological studies to ascertain the routes of infection into the cell will all no doubt contribute to developments in this field.

ACKNOWLEDGMENTS

We thank Jani Seitsonen, Harri Jäälinoja, and Shabih Shakeel for invaluable discussions, Peter Mertens for his critical comments on the manuscript, Mohamed Jaffer and Sean Karriem at UCT and Jacky Welgemoed at Deltamune Roodeplaat for skillful technical support, Hong Zhou for the BTV reconstruction, Jyrki Hokkanen for graphics, and the CSC for access to supercomputer facilities.

This work was supported by the Academy of Finland Center of Excellence Programme in Virus Research (2006–2011; grant 129684 to S.J.B.). V.M. is a fellow of the VGSB.

REFERENCES

1. **Adrian M, Dubochet J, Lepault J, McDowall AW.** 1984. Cryo-electron microscopy of viruses. Nature **308**:32–36.
2. **Basak AK, Gouet P, Grimes J, Roy P, Stuart D.** 1996. Crystal structure of the top domain of African horse sickness virus VP7: comparisons with bluetongue virus VP7. J. Virol. **70**:3797–3806.
3. **Belhouchet M, et al.** 2011. Detection of a fourth orbivirus non-structural protein. PLoS One **6**:e25697. doi:10.1371/journal.pone.0025697.
4. **Bentley L, Fehrsen J, Jordaan F, Huismans H, du Plessis DH.** 2000. Identification of antigenic regions on VP2 of African horsesickness virus serotype 3 by using phage-displayed epitope libraries. J. Gen. Virol. **81**: 993–1000.
5. **Bremer CW.** 1976. A gel electrophoretic study of the protein and nucleic acid components of African horsesickness virus. Onderstepoort J. Vet. Res. **43**:193–200.
6. **Bremer CW, Huismans H, Van Dijk AA.** 1990. Characterization and cloning of the African horsesickness virus genome. J. Gen. Virol. **71**:793–799.
7. **Burrage TG, Trevejo R, Stone-Marschat M, Laegreid WW.** 1993. Neutralizing epitopes of African horsesickness virus serotype 4 are located on VP2. Virology **196**:799–803.
8. **Burroughs JN, et al.** 1994. Purification and properties of virus particles, infectious subviral particles, cores and VP7 crystals of African horsesickness virus serotype 9. J. Gen. Virol. **75**:1849–1857.
9. **Carrillo-Tripp M, et al.** 2009. VIPERdb2: an enhanced and web API enabled relational database for structural virology. Nucleic Acids Res. **37**: D436–D442.
10. **Castillo-Olivares J, et al.** 2011. A modified vaccinia Ankara virus (MVA) vaccine expressing African horsesickness virus (AHSV) VP2 protects against AHSV challenge in an IFNAR−/− mouse model. PLoS One **6**:e16503. doi:10.1371/journal.pone.0016503.
11. **Chen JZ, et al.** 2009. Molecular interactions in rotavirus assembly and uncoating seen by high-resolution cryo-EM. Proc. Natl. Acad. Sci. U. S. A. **106**:10644–10648.
12. **Coetzer JA, Erasmus BJ.** 1994. African horsesickness, p 460–475. *In* Coetzer JA, Thomson CR, Tustin RC (ed), Infectious disease of livestock with special reference to southern Africa, vol 1. Oxford University Press, Oxford, United Kingdom.
13. **Darpel KE, et al.** 2011. Saliva proteins of vector *Culicoides* modify structure and infectivity of bluetongue virus particles. PLoS One **6**:e17545. doi:10.1371/journal.pone.0017545.
14. **Diprose JM, et al.** 2001. Translocation portals for the substrates and products of a viral transcription complex: the bluetongue virus core. EMBO J. **20**:7229–7239.
15. **du Plessis M, Cloete M, Aitchison H, Van Dijk AA.** 1998. Protein aggregation complicates the development of baculovirus-expressed African horsesickness virus serotype 5 VP2 subunit vaccines. Onderstepoort J. Vet. Res. **65**:321–329.
16. **Erasmus BJ.** 1973. The pathogenesis of African horsesickness, p 1–11. *In* Bryans JT, Gerber H (ed), Proceedings of the Third International Conference on Equine Infectious Diseases. Equine infectious diseases, vol III. S. Karger, Basel, Switzerland.
17. **Firth AE.** 2008. Bioinformatic analysis suggests that the orbivirus VP6 cistron encodes an overlapping gene. Virol. J. **5**:48.
18. **Forzan M, Marsh M, Roy P.** 2007. Bluetongue virus entry into cells. J. Virol. **81**:4819–4827.
19. **Forzan M, Wirblich C, Roy P.** 2004. A capsid protein of nonenveloped bluetongue virus exhibits membrane fusion activity. Proc. Natl. Acad. Sci. U. S. A. **101**:2100–2105.
20. **Gouet P, et al.** 1999. The highly ordered double-stranded RNA genome of bluetongue virus revealed by crystallography. Cell **97**:481–490.
21. **Goujon M, et al.** 2010. A new bioinformatics analysis tools framework at EMBL-EBI. Nucleic Acids Res. **38**:W695–W699.
22. **Grimes JM, et al.** 1998. The atomic structure of the bluetongue virus core. Nature **395**:470–478.
23. **Grubman MJ, Lewis SA.** 1992. Identification and characterization of the structural and nonstructural proteins of African horsesickness virus and determination of the genome coding assignments. Virology **186**:444–451.
24. **Harauz G, van Heel M.** 1986. Similarity measures between images. Exact filters for general geometry of 3D reconstructions. Optik **73**:146–156.
25. **Hassan SH, Wirblich C, Forzan M, Roy P.** 2001. Expression and functional characterization of bluetongue virus VP5 protein: role in cellular permeabilization. J. Virol. **75**:8356–8367.
26. **Hassan SS, Roy P.** 1999. Expression and functional characterization of bluetongue virus VP2 protein: role in cell entry. J. Virol. **73**:9832–9842.
27. **Hewat EA, Booth TF, Roy P.** 1992. Structure of bluetongue virus particles by cryoelectron microscopy. J. Struct. Biol. **109**:61–69.
28. **Hewat EA, Booth TF, Wade RH, Roy P.** 1992. 3-D reconstruction of bluetongue virus tubules using cryoelectron microscopy. J. Struct. Biol. **108**:35–48.
29. **Heymann JB.** 2001. Bsoft: image and molecular processing in electron microscopy. J. Struct. Biol. **133**:156–169.

30. **Howell PG.** 1960. The 1960 epizootic of African horsesickness in the Middle East and SW Asia. J. South Afr. Vet. Assoc. **31**:329–335.
31. **Howell PG.** 1962. The isolation and identification of further antigenic types of African horsesickness virus. Onderstepoort J. Vet. Res. **29**:139–149.
32. **Huiskonen JT, et al.** 2006. Structure of the bacteriophage π6 nucleocapsid suggests a mechanism for sequential RNA packaging. Structure **14**: 1039–1048.
33. **Huismans H, van der Walt NT, Cloete M, Erasmus BJ.** 1987. Isolation of a capsid protein of bluetongue virus that induces a protective immune response in sheep. Virology **157**:172–179.
34. **Jäälinoja HT, Huiskonen JT, Butcher SJ.** 2007. Electron cryomicroscopy comparison of the architectures of the enveloped bacteriophages π6 and π8. Structure **15**:157–167.
35. **Larkin MA, et al.** 2007. Clustal W and Clustal X version 2.0. Bioinformatics **23**:2947–2948.
36. **Lubroth J.** 1988. African horsesickness and the epizootic in Spain 1987. Equine Pract. **10**:26–33.
37. **Lupas A, Van Dyke M, Stock J.** 1991. Predicting coiled coils from protein sequences. Science **252**:1162–1164.
38. **Marchi PR, et al.** 1995. Proteolytic cleavage of VP2, an outer capsid protein of African horsesickness virus, by species-specific serum proteases enhances infectivity in *Culicoides*. J. Gen. Virol. **76**:2607–2611.
39. **Martinez-Torrecuadrada JL, Casal JI.** 1995. Identification of a linear neutralization domain in the protein VP2 of African horsesickness virus. Virology **210**:391–399.
40. **Matsuo E, Celma CC, Roy P.** 2010. A reverse genetics system of African horsesickness virus reveals existence of primary replication. FEBS Lett. **584**:3386–3391.
41. **McIntosh BM.** 1958. Immunological types of horsesickness virus and their significance in immunization. Onderstepoort J. Vet. Res. **27**:465–538.
42. **Meiswinkel R, Paweska JT.** 2003. Evidence for a new field *Culicoides* vector of African horsesickness in South Africa. Prev. Vet. Med. **60**:243–253.
43. **Meiswinkel R, van Rijn P, Leijs P, Goffredo M.** 2007. Potential new *Culicoides* vector of bluetongue virus in northern Europe. Vet. Rec. **161**: 564–565.
44. **Mellor PS.** 1992. Culicoides as potential orbivirus vectors in Europe, p 278–283. *In* Walton E, Osburn BI (ed), Bluetongue, African horsesickness, and related orbiviruses. CRC Press Inc, Boca Raton, FL.
45. **Mellor PS, Boorman J, Baylis M.** 2000. *Culicoides* biting midges: their role as arbovirus vectors. Annu. Rev. Entomol. **45**:307–340.
46. **Mellor PS, Carpenter S, White DM.** 2009. Bluetongue virus in the insect host, p 295–320. *In* Mellor PSB, et al (ed), Bluetongue. Elsevier, Paris, France.
47. **Mellor PS, Hamblin C.** 2004. African horsesickness. Vet. Res. **35**:445–466.
48. **Mellor PS, Pitzolis G.** 1979. Observations on breeding sites and light-trap collections of *Culicoides* during an outbreak of bluetongue in Cyprus. Bull. Entomol. Res. **69**:229–234.
49. **Mirchamsy H, Hazrati A.** 1973. A review of the aetiology and pathology of African horsesickness. Arch. Hessarek Iran **25**:23–46.
50. **Naitow H, Tang J, Canady M, Wickner RB, Johnson JE.** 2002. L-A virus at 3.4 Å resolution reveals particle architecture and mRNA decapping mechanism. Nat. Struct. Biol. **9**:725–728.
51. **Nason EL, et al.** 2004. Interactions between the inner and outer capsids of bluetongue virus. J. Virol. **78**:8059–8067.
52. **Needleman SB, Wunsch CD.** 1970. A general method applicable to the search for similarities in the amino acid sequence of two proteins. J. Mol. Biol. **48**:443–453.
53. **Oellermann RA.** 1970. Plaque formation by African horsesickness virus and characterization of its RNA. Onderstepoort J. Vet. Res. **37**:137–143.
54. **Pettersen EF, et al.** 2004. UCSF Chimera—a visualization system for exploratory research and analysis. J. Comput. Chem. **25**:1605–1612.
55. **Potgieter AC, et al.** 2009. Improved strategies for sequence-independent amplification and sequencing of viral double-stranded RNA genomes. J. Gen. Virol. **90**:1423–1432.
56. **Purse BV, et al.** 2005. Climate change and the recent emergence of bluetongue in Europe. Nat. Rev. Microbiol. **3**:171–181.
57. **Rafyi A.** 1961. Horse sickness. Bull. Off. Int. Epizoot. **56**:216–250.
58. **Reinisch KM, Nibert ML, Harrison SC.** 2000. Structure of the reovirus core at 3.6 Å resolution. Nature **404**:960–967.
59. **Roy A, Kucukural A, Zhang Y.** 2010. I-TASSER: a unified platform for automated protein structure and function prediction. Nat. Protoc. **5**:725–738.
60. **Roy P, Bishop DH, Howard S, Aitchison H, Erasmus B.** 1996. Recombinant baculovirus-synthesized African horsesickness virus (AHSV) outer-capsid protein VP2 provides protection against virulent AHSV challenge. J. Gen. Virol. **77**:2053–2057.
61. **Roy P, Mertens PP, Casal I.** 1994. African horsesickness virus structure. Comp. Immunol. Microbiol. Infect. Dis. **17**:243–273.
62. **Scanlen M, Paweska JT, Verschoor JA, van Dijk AA.** 2002. The protective efficacy of a recombinant VP2-based African horsesickness subunit vaccine candidate is determined by adjuvant. Vaccine **20**:1079–1088.
63. **Seitsonen J, et al.** 2010. Interaction of alphaVbeta3 and alphaVbeta6 integrins with human parechovirus 1. J. Virol. **84**:8509–8519.
64. **Stone-Marschat MA, et al.** 1996. Immunization with VP2 is sufficient for protection against lethal challenge with African horsesickness virus type 4. Virology **220**:219–222.
65. **Theiler A.** 1921. African horse sickness (pestis equorum). South Afr. Dept. Agric. Sci. Bull. **19**:30.
66. **Thiry E, et al.** 2006. Bluetongue in northern Europe. Vet. Rec. **159**:327.
67. **van Staden V, Huismans H.** 1991. A comparison of the genes which encode non-structural protein NS3 of different orbiviruses. J. Gen. Virol. **72**:1073–1079.
68. **van Staden V, Theron J, Greyling BJ, Huismans H, Nel LH.** 1991. A comparison of the nucleotide sequences of cognate NS2 genes of three different orbiviruses. Virology **185**:500–504.
69. **Venter GJ, Wright IM, Van Der Linde TC, Paweska JT.** 2009. The oral susceptibility of South African field populations of *Culicoides* to African horsesickness virus. Med. Vet. Entomol. **23**:367–378.
70. **Wilson A, Mellor PS, Szmaragd C, Mertens PP.** 2009. Adaptive strategies of African horsesickness virus to facilitate vector transmission. Vet. Res. **40**:16.
71. **Yan X, Sinkovits RS, Baker TS.** 2007. AUTO3DEM—an automated and high throughput program for image reconstruction of icosahedral particles. J. Struct. Biol. **157**:73–82.
72. **Zhang X, et al.** 2010. Bluetongue virus coat protein VP2 contains sialic acid-binding domains, and VP5 resembles enveloped virus fusion proteins. Proc. Natl. Acad. Sci. U. S. A. **107**:6292–6297.
73. **Zhang X, et al.** 2008. Near-atomic resolution using electron cryomicroscopy and single-particle reconstruction. Proc. Natl. Acad. Sci. U. S. A. **105**:1867–1872.
74. **Zhang Y.** 2008. I-TASSER server for protein 3D structure prediction. BMC Bioinformatics **9**:40. doi:10.1186/1471-2105-9-40.